Assessment of the Information Content in Solar Reflective Satellite Measurements with respect to Crop Growth Model State Variables

Nathaniel Levitan[1], Barry Gross[1,2]

[1]Dept, of Electrical Engineering, City College of New York, 160 Convent Ave, New York, NY

[2]NOAA-CREST, 160 Convent Ave, New York, NY

A paper from the Proceedings of the
14th International Conference on Precision Agriculture
June 24 – June 27, 2018
Montreal, Quebec, Canada

Abstract. *To increase the utilization of satellite remote sensing data in precision agriculture, it is necessary to retrieve the most relevant variables from the satellite signals so that the retrievals can be directly utilized by agricultural management entities. The variables that make up the state vector description of existing crop growth models provide inherent relevance to on-farm decision making because they can be used to predict future crop status based on changing farm inputs. In this study, the information content of MODIS spectral surface reflectance measurements with respect to the state variables in the STICS crop growth model for maize is analyzed. Specifically, it is shown that the MODIS measurements can predict the state variables of an ensemble average of STICS crop growth simulations with R^2 values of up to 0.75 using a bidirectional long short-term memory (BLSTM) network. The analysis is performed using a training, validation, test data division scheme typical in machine learning using county-median measurements from 36 counties across the United States; data from 2006, 2008, 2010, 2012, and 2014 is used for training, data from 2005, 2009, and 2011 is used for validation and data from 2007 and 2013 is used for testing. Significant correlation of the harvested organ biomass, subsurface soil water, and phenological stage state variables with the MODIS measurements is shown in this study, implying that the remote sensing signal can be used for significantly more than for retrieving the leaf area index.*

Keywords.
Crop Growth Models. STICS, MODIS, BLSTM.

Introduction

Coupling remote sensing measurements with crop growth models (CGMs) has long been an objective of the agronomy and remote sensing communities (Yuping, et al., 2008) (Ines, Das, Hansen, & Njoku, 2013) (Fang, Liang, Hoogenboom, Teasdale, & Cavigelli, 2008) (Weiss, et al., 2001) (Machwitz, et al., 2014) (Thorp, et al., 2012) (Zhang, et al., 2016) (Lobell, Thau, Seifert, Engle, & Little, 2015) (Jin, Azzari, & Lobell, 2017). Incorporating crop growth modelling into remote sensing retrievals has the potential to reduce the uncertainty in the retrievals by introducing the constraints on the growth dynamics imposed by the biology. Further, the description of the vegetation state retrieved by coupling crop growth models is potentially more useful to the precision agriculture community because it can be directly used in a CGM to model the response of the crop to changes in the agromanagment practices and climate. Unfortunately, there have been difficulties in coupling remote sensing measurements with CGMs because:

a.) Canopy radiative transfer inversion algorithms have great challenges retrieving variables beyond the leaf area index (LAI) from the top-of-canopy solar reflectances, and
b.) It is difficult to construct a model that relates the CGM state variables and the top-of-canopy solar reflectances, and
c.) Microwave-based measurements, such as those of surface soil moisture, generally have a very coarse pixel size (tens of kilometers) or very low revisit times that limits their precision agriculture applications

The difficulty in retrieving more variables than the LAI occurs because the level of ill-posedness in the canopy radiative transfer (RT) inversion problem rises quickly as one attempts to retrieve more variables (Baret, Houlès, & Guérif, 2007) (Combal, et al., 2003) without the mechanistic constraint of the growth dynamics. As a result, the LAI is often the only solar-reflective remote sensing retrieval coupled to the crop growth models (Ines, Das, Hansen, & Njoku, 2013) (Fang, Liang, Hoogenboom, Teasdale, & Cavigelli, 2008). While some studies have used complex regularization techniques to expand the inversion of the canopy RT models to other variables, such as leaf chlorophyll content (Houborg, et al., 2015), there are large uncertainties in these retrievals and even with these additional variables it is still difficult to form a complete understanding of the vegetation state to perform a simulation in a CGM from these parameters alone.

To incorporate more variables into the coupling between remote sensing measurements and CGMs, it is necessary to robustly relate the CGM state variables and the top-of-canopy solar reflectances. In the literature, attempts to do so have been made by using empirical relationships to connect CGM state variable and canopy RT model inputs; the field-derived linear relationship between leaf chlorophyll content and leaf nitrogen content is one example of a relationship that can be used for this coupling (Schlemmer, et al., 2013). Several studies (Machwitz, et al., 2014) (Weiss, et al., 2001) (Thorp, et al., 2012) (Zhang, et al., 2016) have attempted to perform coupling using similar empirical relationships; however, these approaches suffer from both the inaccuracies in the empirical relationships and the need to use estimated *a priori* values for some of the canopy RT inputs that cannot be determined from the CGMs. This limits the generalizability and global applicability of these model couplings because the amount of field data used to construct these empirical relationships is inherently limited by cost and, as a result, the relationships may significantly vary from site-to-site, potentially causing large errors in the CGM-canopy RT model coupling.

Overview

In order to fully utilize solar reflective remote sensing measurements of crop growth for precision agriculture, it is desirable to have a way of directly connecting the top-of-canopy reflectance measurements to the state vector of a CGM. It is critical for this relationship to be broadly applicable over multiple regions and different growing season conditions in order to allow it to be broadly used in precision agriculture. Machine learning is well-suited to solve these types

of problems where a generalizable relationship needs to be learned from large amounts of existing remote sensing data. In this study, it is sought to show that it is feasible to learn a relationship between the CGM vegetation state vector and the remote sensing reflectances via machine learning techniques. To do so, the STICS CGM agromanagment parameters are varied to generate an ensemble average of maize simulations in 36 different counties in the United States between 2005 and 2014. Then, MODIS county-median maize surface reflectances for the county-years simulated with STICS are obtained and bidirectional long short-term memory (BLSTM) networks are used to understand how well the MODIS surface reflectances can predict the ensemble average of the state variables of the STICS simulations.

Data

The MCD43A4.005 BRDF-adjusted nadir surface reflectance product is used to obtain surface reflectances in seven 500 meter MODIS solar-reflective bands: 620 – 670 nm, 841 – 876 nm, 545 -565 nm, 1230 – 1250 nm, 1628 – 1652 nm and 2105 – 2155 nm. Only pixels that are more than 90 % covered by maize are considered in this study; the 30 m USDA Crop Data Layer is analyzed using the gdalwarp (McInerney & Kempeneers, 2014) command-line utility to identify MODIS 500 m pixels that are more than 90 % covered in maize. The daily county-level median of each MODIS surface reflectance bands is used in the BLSTM-based analysis for county-years that have more than fifty 500 m MODIS pixels that are more than 90 % covered in maize.

The counties used in this study were randomly selected from those that had more than 80,000 acres of maize harvested and less that 15 % of maize irrigated according to the USDA NASS Farm and Ranch Irrigation Survey from 2007 (National Agricultural Statistics Service, 2017), accessed through the QuickStats service (quickstats.nass.usda.gov). Only counties that were predominantly non-irrigated were used to remove the unknown irrigation agromanagment parameter from the CGM simulations; it is assumed that these counties are rainfed and the irrigation value is thus set to zero in the CGM. Data is obtained from 2005 to 2014; however, the USDA Crop Data Layer did not have national coverage until the 2008 season, so fewer counties are used before 2008. Figure 1 illustrates the counties selected and the number of points per county.

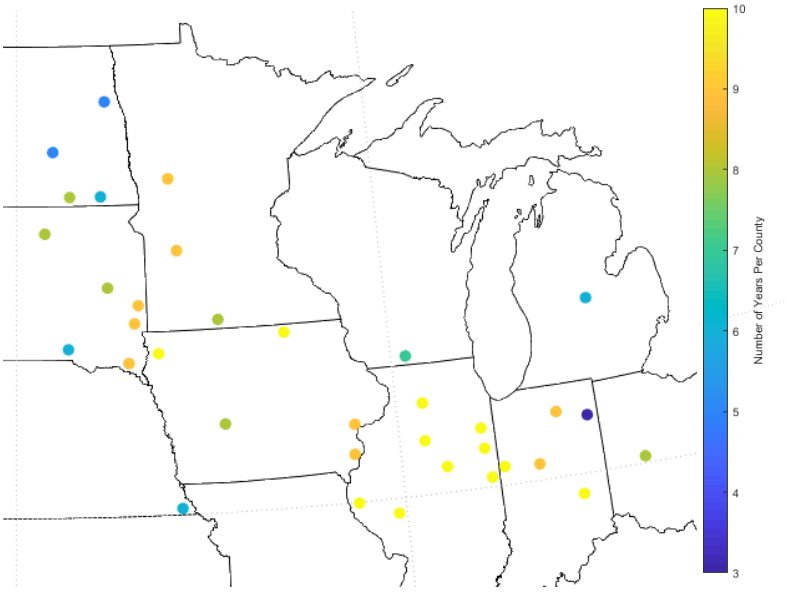

Fig 1. Counties used for analysis and number of years of MODIS data used per county

The data was divided into training, validation, and test divisions by year for analysis by the BLSTMs, as will be described further in section V. The years for each data division and number of county-years per division are listed in Table 1. The number of county-years represents the total number of different growing seasons in each data division; if 5 years of data for 2 counties were

used, this would represent 10 county-years of data.

Table 1. Number of county-years in each data division

Data Division	Years	Number of county-years
Training	2006, 2008, 2010, 2012, 2014	157
Validation	2005, 2009, 2011	77
Test	2007, 2013	66

In order to run the crop-growth model simulations, the 1-degree NASA POWER agroclimatology dataset (Stackhouse, Westberg, Chandler, Zhang, & Hoell, 2017) is used. The dataset contains all the necessary agrometeorological data to run the STICS CGM. Furthermore, in order to validate the methodology of using the CGM to generate an ensemble of vegetation state variables, the yields predicted by it are compared against the annual county-level yields determined through National Agricultural Statistics Service surveys, also accessed through the QuickStats service.

Methods

STICS crop growth model simulations

For each county-year, an ensemble of vegetation state variables are simulated using the STICS CGM (Brisson, et al., 2002) by varying the agromanagment parameters and using the local meteorology from the NASA POWER dataset. The varied parameters are listed in Table 2; all combinations of parameters are simulated, leading to a total of 320 simulations per county-year. The values simulated for variety planted represent all 16 maize varieties prepackaged with the STICS models, while only one value (the STICS default) was simulated for fertilizer applied because the STICS default soil properties (as opposed to a soil survey data) are used and it would be difficult for the model to truly simulate nitrogen processes in the soil without knowing the true soil properties. The sowing dates and planting densities simulated are similar to those used in a recent maize remote sensing study (Lobell, Thau, Seifert, Engle, & Little, 2015), which uses a similar approach to generating an ensemble average of crop simulations (albeit for a different purpose).

After performing the simulations, the average of the state variables of the simulations for each county-year is calculated to find an ensemble state vector. For all variables except the phenology, this is done by simply take the numerical mean for each variable for each day for each county year. For the phenology state variable, which stores the phenological state of the crop in the simulation, the percentage of simulation runs in each phenological state for each day for each county year is calculated instead; this makes the discrete phenological state variable amiable to analysis by machine learning classification approaches.

Table 2. Agromanagment parameters varied to generate ensemble of STICS CGM simulations for each county-year

Parameter Name	Units	Values Simulated
Variety planted	N/A	Clarica, Magrite, Banguy, DK240, DK312, Anjou285, DK300, Nobilis-DE, DK604, Cecilia, Volga, Dunia, Furio, Cherif, Pactol, DK250
Fertilizer Applied	kg N/ha	220
Sowing Date	Days Since January 1st	105 (April 14-15), 115 (April 25-26), 125 (May 4-5), 135 (May 14 -15), 145 (May 24 – 25)
Planting Density	Plants per m^2	4.5, 6, 7.5, 9

BLSTMs

Long short-term memory networks (LSTMs) are recurrent neural networks that can be used to predict an output time series of any number of variables from an input time series of any number of variables; these networks have proven to be extremely valuable (Greff, Srivastava, Koutník, Steunebrink, & Schmidhuber, 2017) for time series machine learning. In this study, a variant of a bidirectional variant of LSTMs, called BLSTMs (Weninger, Bergmann, & Schuller, 2015), is used to perform the analysis; this variant has the advantage of being able to use information from both the future and the past to make predictions. To understand how well remote sensing

measurements can be connected the CGM state variables, two BLSTMs are trained to predict the ensemble CGM state variable mean from the MODIS surface reflectances: one BLSTM is used to predict the phenological state variables and another is used for all other state variables. Two separate BLSTMs are used because different cost functions and layers need to be used for physical quantities and phenological class member probabilities. A sum of square error cost function is appropriate for physical quantities while a cross-entropy cost function is appropriate for probabilities, which also leads to the choice of a linear output layer (which allows for any value of the outputs) for the physical quantities and a softmax output layer (which guarantees that the outputs are probabilities that sum up to 1) for the phenological class member probabilities.

The structure of the two networks is illustrated in Figures 2 and 3. Both networks have inputs of the MODIS BRDF-adjusted nadir surface reflectance in seven bands; however, the phenological BLSTM (Figure 3) also has two meterological variables (the normalized thermal time and the incoming solar radiation) as inputs due to the critical dependence of the phenological state on meterological conditions. The incoming solar radiation is taken directly from the NASA POWER dataset while the normalized thermal time is calculated as

$$Normalized\ Thermal\ Time(t) = TT(t)/TT(December\ 31st) \quad (1)$$

$$TT(t) = \int_0^t \max\left(\frac{T_{max}(t\prime)+T_{min}(t\prime)}{2} - 6{,}0\right) dt' \quad (2)$$

where t is in days since February 15th, T_{max} is the daily maximum temperature, and T_{min} is the daily minimum temperature. T_{max} and T_{min} are taken from the NASA POWER dataset.

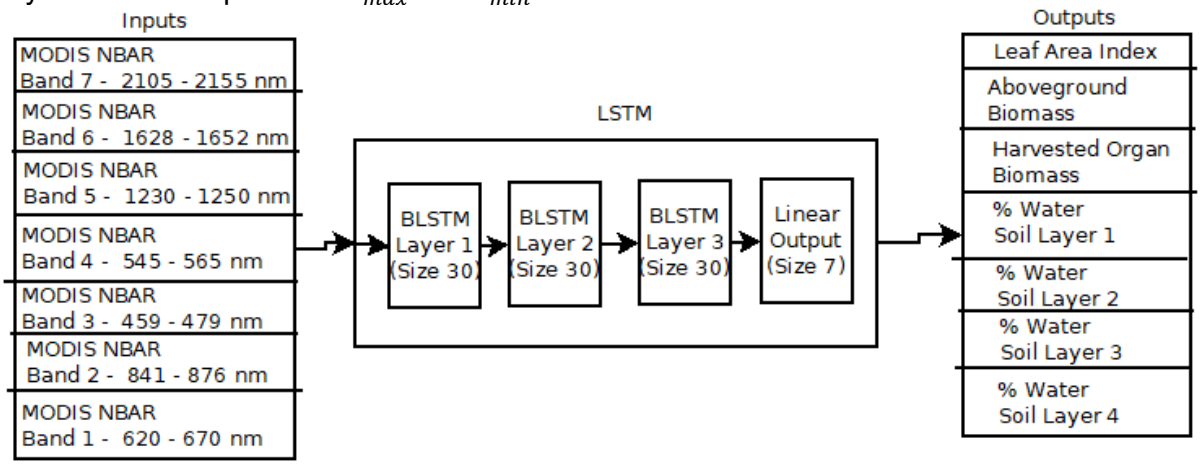

Fig 2. BLSTM for physical state variables

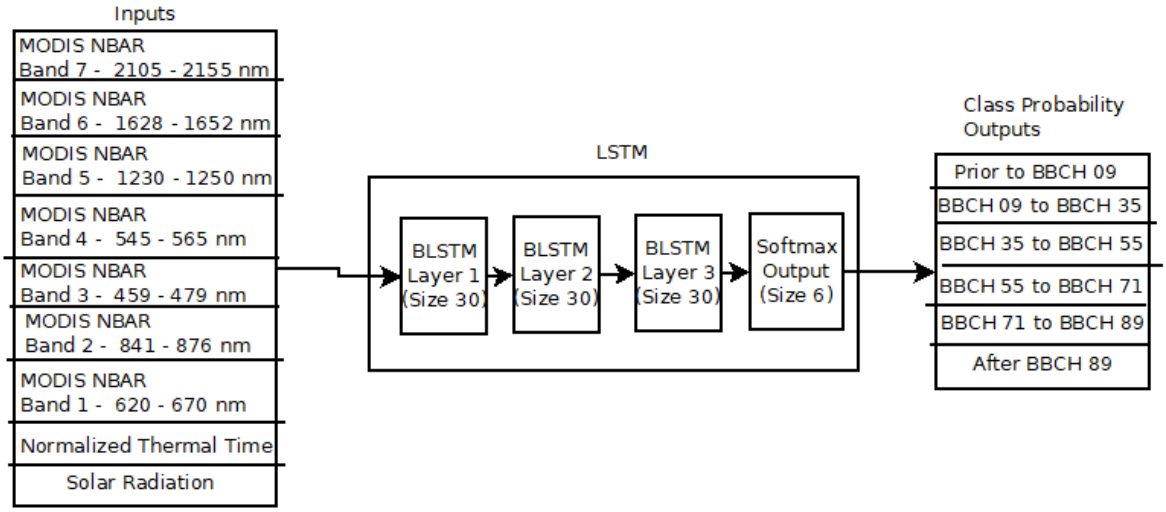

Fig 3. BLSTM for phenological class member probabilities state variables

The physical state variable BLSTM is trained to predict seven state variables selected from

the STICS model. The physical state variables selected are those that are most likely to be predicted accurately by a model using meterological information to simulate yield processes. The leaf area index was selected because of its importance in determining canopy light interception. The harvested organ biomass was selected because its value at the end of the season represents the crop yield and its in-season values represent the development of the yield. The aboveground biomass was selected because it provides a good representation of the overall growth of the plant and because CGMs are known to perform poorly on the harvest index-type stress calculations that go into calculating the harvested organ biomass (Jin, Azzari, & Lobell, 2017). The soil moisture variables were selected because they are connected to evapotranspiration and precipitation amounts in rainfed maize and thus their dynamic variability can be captured by a mechanistic crop model driven by meterological information (although without soil data, the features in the variability of these variables caused by differences in soil water retention capacity cannot be captured).

Table 3. Phenlogical Stages Predicted by STICS Model During Growing Season, adapted from (Lancashire, et al., 1991)

BBCH Code	Description
BBCH 09	Emergence
BBCH 35	5 nodes detectable (Stem elongation)
BBCH 55	Middle of tassel emergence
BBCH 71	Beginning of grain development, kernels at blister stage
BBCH 89	Fully ripe, post maturity

The phenological state variable BLSTM is trained to predict the probabilities of all the vegetation states predicted by the STICS model during the growing season. The phenological dates predicted by the STICS model are based on a subset of the BBCH system for maize (Lancashire, et al., 1991) and are summarized in Table 2.

Both BLSTMs are trained and evaluated according to the standard training, validation, test data division scheme. Under this scheme, training data is used to train the BLSTM by gradient descent, validation is used to prevent overfitting by stopping the training when the network ceases to improve its performance on the validation data, and test data, which is never exposed to the network in the training phase, is used to evaluate the network's performance and generalization to new data. As indicated in Table 1, each year is only assigned to one of the three data divisions to ensure that the network is generalizable and not over fit.

Results and Discussion

Accuracy of STICS ensemble crop growth model simulations

Prior to analyzing the relationship between the STICS ensemble-average state variables and the MODIS measurements, it is important to consider the accuracy of the STICS simulations and the effects on this study. To do so, the ensemble-average county-level crop yield and crop yield anomaly simulated by STICS are plotted against ground truth values from the USDA NASS county-level crop yields obtained from field surveys. The simulated yield anomaly is calculated by subtracting the simulated yield from the 2005-2014 average of simulated yields for the county, while the actual yield anomaly is calculated by subtracting the actual yield from the 2005-2014 average of simulated yields for the county. The scatterplots for simulated versus actual yield and yield anomaly are shown in Figure 4a-b; all county-years for which the STICS model was run for 2005-2014 are used in the analysis.

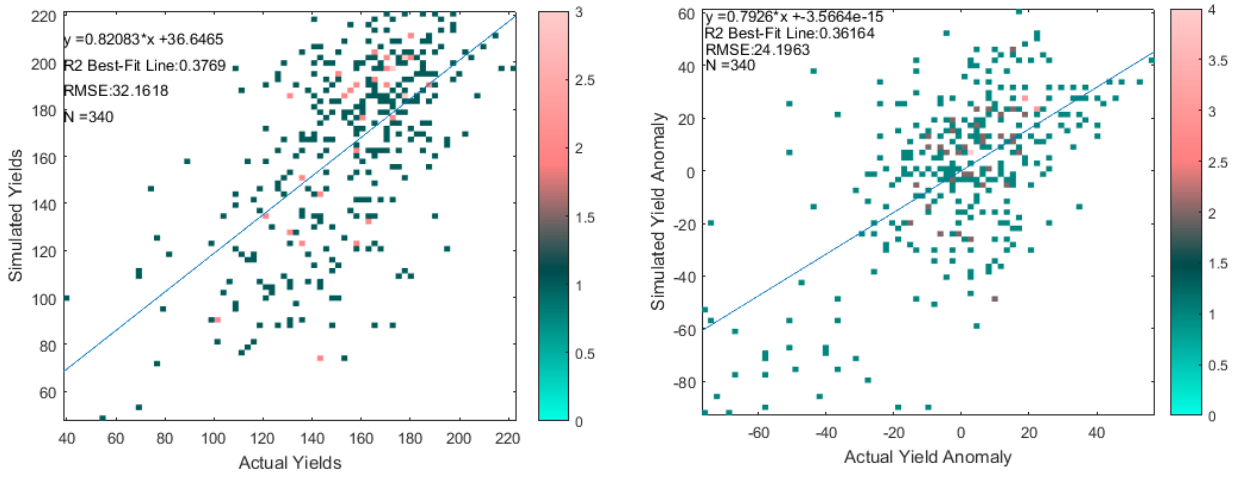

Fig 4. STICS ensemble average simulated versus actual USDA NASS (a) yield and (b) yield anomaly in bu/acre. Colorbar represents number of points per pixel

In figure 4, one can see that STICS ensemble average is correlated with the actual USDA NASS yield with an R^2 value of 0.38 and the actual USDA NASS yield anomaly with an R^2 value of 0.36. While these R^2 values appear low, it is important to note that it is difficult to use a crop growth model to accurately simulate the yield in the absence of knowledge of the local agromanagment parameters. For example, a recent study (Morell, et al., 2016) that attempted to use estimates of regional agromanagment parameters and soil properties from available data sources and expert knowledge by local agronomists to predict the crop yield using the HybridMaize CGM was only able to predict the county-level crop yield with an R^2 of 0.52 for the yield anomaly. The R^2 compares favorably to the performance of this study considering that this study avoids making any estimates of the regional agromanagment parameters because of their very large uncertainties. Therefore, it is difficult to obtain a large dataset of collocated 500 m MODIS observations and CGM simulations at significantly higher level of simulation accuracy, although we plan to address this issue in future work using agromanagment data from university and government research plots along with high resolution Landsat data. The results of this study are important to establish the feasibility of retrieving the CGM state variables from solar reflective multispectral satellite data and encourage collaborations to collect more geolocated agromanagment data to train, validate and test such algorithms. While the STICS ensemble average can only be thought of as an estimate of the vegetation state, identifying a robust correlation between the ensemble and the MODIS measurement that holds outside of the years in which it was identified strongly implies that the physical forcing applied by the meteorology on the crop is detectable in the top-of-canopy reflectance signal.

Ability of MODIS measurements to predict STICS ensemble average

In this section, the ability of the MODIS measurements to predict the STICS ensemble average is evaluated. To do so, the performance of the two BLSTMs described in section V on test data, namely the county-years from 2007 and 2013, is evaluated. In figure 5, the performance of the BLSTM for the non-phenological state variables for the test data is displayed. In figure 5a, the R^2 coefficient between the actual STICS state variable value and the BLSTM predicted state variable is shown at each normalized thermal time (normalized thermal time is defined in equation 1).The R^2 coefficients are calculated for each state variable by interpolating the daily actual STICS state variables and BLSTM predictions to a normalized thermal time grid and then calculating the R^2 coefficient between the actual value and prediction at each discrete grid point (100 discrete points between normalized thermal times of 0.01 and 0.99). Calculating the R^2 coefficients independently at each normalized thermal time serves to remove the effects of the mean training dynamics from the calculation and only analyze the intersite retrieval performance (a significantly more challenging task than retrieving the mean dynamics). In figure 5b, the root mean square error (RMSE) of the BLSTM predicted state variable at each normalized thermal time is displayed

as a percentage of the standard deviation of the actual STICS state variable at that normalized thermal time across all test sites. The interpolation on the normalized thermal grid is done identically as in Figure 5a. The limits of the color bar in figure 5 are set such that only percentages below 100 % are displayed in a color other than dark red; the segments not in dark red represent the times at which individual state variables are well retrieved by the BLSTM.

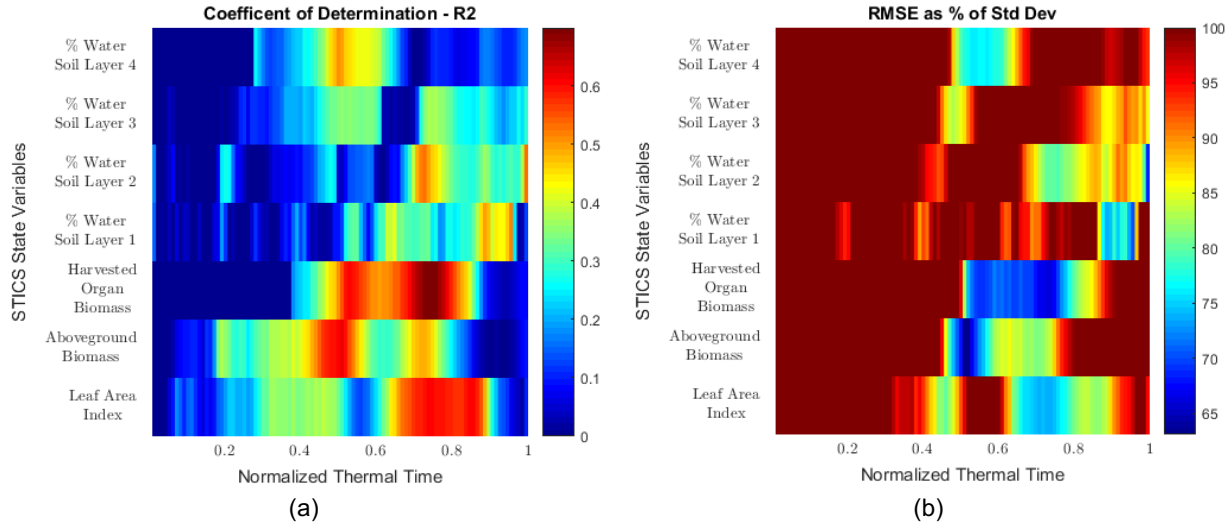

Fig 5. Performance for BLSTM for non-phenological state variables on test dataset (2007 and 2013) as measured by (a) the coefficient of determination – R2 and (b) RMSE as a percentage of standard deviation

In figure 5, the harvested organ biomass is seen to be the variable best retrieved by the BLSTM. Its predictions by the BLSTM are seen to be correlated across all test sites with an R^2 coefficient above 0.6 for a significant portion of the growing season and the RMSE of its prediction is often below 75 % of the mean during this time. The LAI is the next best retrieved variable, with an R^2 coefficient around 0.6 for a decent amount of time in the growing season, but significantly less than the harvested organ biomass. While it may seem surprising that the harvested organ biomass is better correlated than the LAI despite the focus on retrieving the LAI in canopy RT inversion studies, one needs to consider both that MODIS measurements have been found to be significantly correlated with the crop yield in previous studies (Sakamoto, Gitelson, & Arkebauer, 2013) (Johnson, 2016) and that the performance of the retrievals in this study are being assessed after the mean dynamics have been removed. Canopy RT inversion studies generally calculate their retrieval performance statistics using one scatterplot for all times; however, a significant portion of the variability of LAI is explained by the mean LAI dynamics (Koetz, Baret, Poilve, & Hill, 2005) and this study seeks to assess the performance of retrieving LAI once the mean dynamics have been removed. In addition, the soil water in the root zone are seen to be significantly correlated with the measurements in Figure 5 with R^2 coefficients between 0.4 and 0.5; this can be seen as the effect of the effects of the meteorology (precipitation, potential evapotranspiration, etc.) on the water status of the entire plant-soil system that has an effect on both the STICS simulations and the MODIS measurements, causing a correlation between the soil water state variables and the MODIS measurements. The correlation of soil moisture agrees with previous studies that found correlation of soil moisture below maize canopies to the plant vegetation indices, and consequently to the top-of-canopy reflectance signal (Swain, Wardlow, Sunil, Rundquist, & Hayes, 2013).

We now turn to analyzing the performance of the BLSTM for retrieving the STICS ensemble average phenology from the MODIS reflectances. First, in figure 6, using the same methodology as for Figure 5a, the coefficient of determination (R^2) between the BLSTM-predicted phenological class membership probabilities and the actual STICS ensemble average class membership probabilities is plotted.

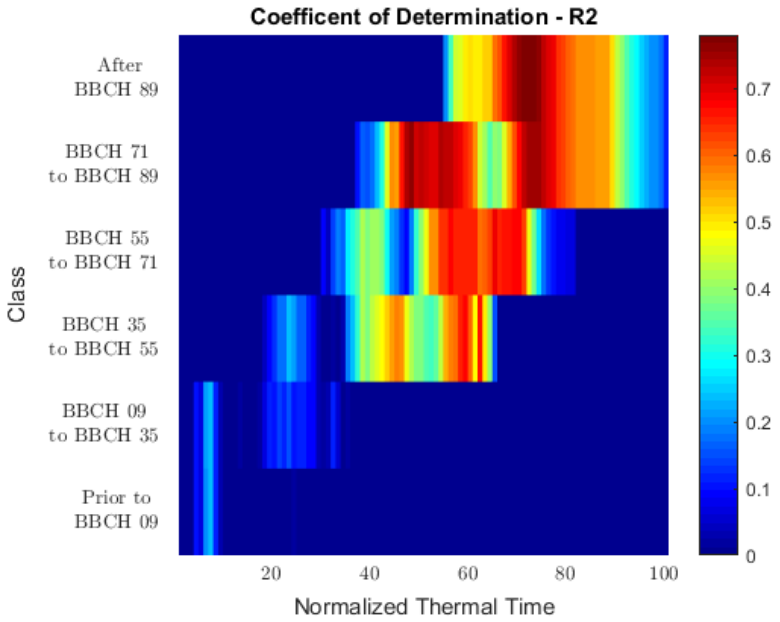

Fig 6. Coefficient of determination (R2) for BLSTM for phenology state variables on test dataset (2007 and 2013)

In figure 6, it is shown that four (BBCH 35 to 55, BBCH 55 to 71, BBCH 71 to 89, and After BBCH 89) of the BLSTM-predicted phenological class membership probabilities are well correlated with the actual probabilities, often with an R^2 value above 0.6. Because figure 6 is on a normalized thermal time grid and the R^2 values are calculated independently at each normalized thermal time, the results show that the BLSTM outperforms using the mean training phenological stage for a particular normalized thermal time with quite large R^2 values.

The overall classification accuracy provided by the BLSTM is shown in Figure 7, which shows the confusion matrix for the test dataset on a daily basis. The y-axis represents the BLSTM predicted class, while the x-axis represents the actual STICS ensemble average class. Each box shows the number and percentage of actual classes that were given a particular prediction; as a result, boxes on the green diagonal represent correct classifications while boxes off the diagonal represent incorrect predictions. The percentages in the gray row at the bottom of the figure represent the combined accuracy of making a prediction of a particular actual class, while the gray column represents the combined accuracy of a prediction of a given class. The overall prediction accuracy is given in the purple box.

As seen from figure 7, overall 90% of the days between February 15th and January 1st are classified correctly by the BLSTM, which implies that about 5 days are misclassified per class, which compares favorably to the 6.7 to 7.6 day average error in retrieving the actual phenological dates (rather than the class membership) in (Sakamoto, Gitelson, & Arkebauer, 2013). The retrieval accuracies for the individual classes are also seen in figure 7 and they vary significantly; however, it is notable that even for some classes that have lower accuracy, the correlations in Figure 6 are still high, indicating useful information about the probability of class membership is being retrieved by the BLSTM.

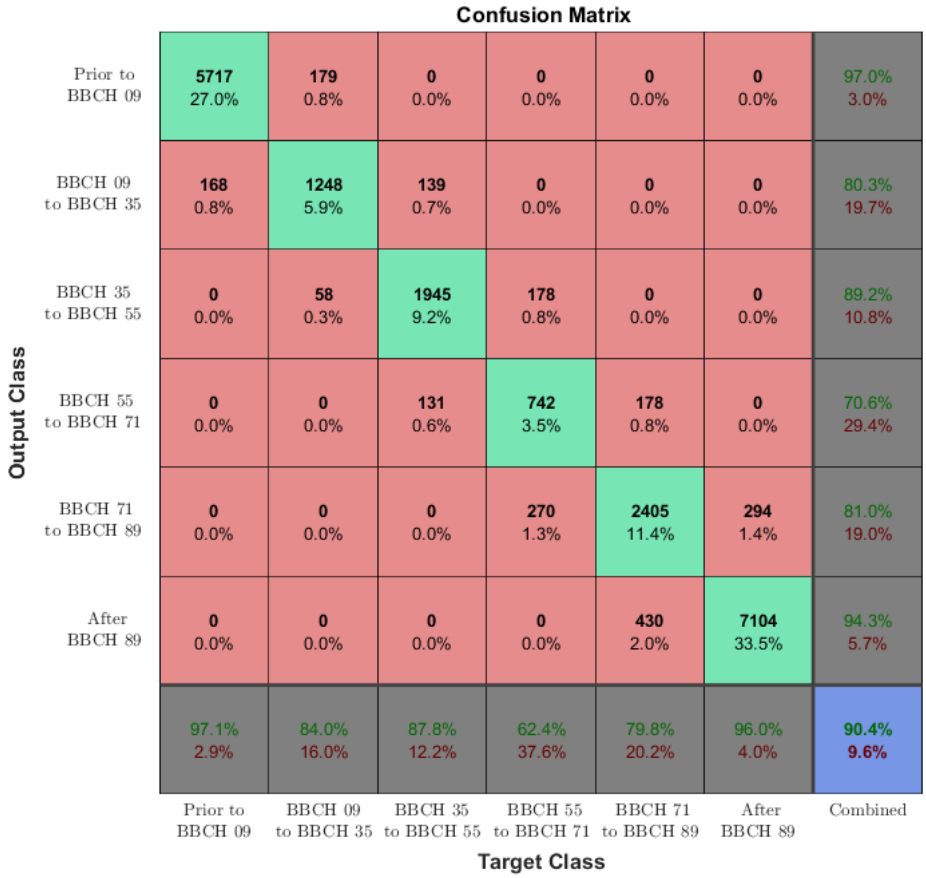

Fig 7. Confusion matrix for BLSTM for phenology state variables on test dataset (2007 and 2013))

Conclusion

Overall, this study showed that the forcings in the STICS crop growth model are captured in MODIS top-of-canopy measurements and that the MODIS measurements consequently have significant potential in being used to retrieve information for assimilation into crop growth models beyond the existing state of the art. Specifically, it was shown that a BLSTM can be used to predict several state variables in the ensemble average of STICS crop growth model simulations run with different agromanagment parameters from the BRDF-adjusted MODIS surface reflectance measurements at the county level. This provides evidence that machine learning can be used to obtain a more complete description of the crop vegetation state than the commonly retrieved leaf area index. Specifically, the harvested organ biomass, the phenological state and plant water status seem to be good candidates to be retrieved from remote sensing in addition to the leaf area index. Further work needs to be done to improve the accuracy of the STICS crop growth simulations by obtaining ground truth datasets of agromanagment parameters in order to build a more realistic machine learning predictor of these state variables; hopefully this current work illustrates the feasibility of such an approach and provides motivation for the community to increase data sharing to allow the potential of machine learning in agricultural remote sensing to be realized.

Acknowledgements

We are grateful to F. Weninger, J. Bergmann, and B. Schuller for publically releasing the CURRENNT LSTM framework under the GPL license at https://sourceforge.net/projects/currennt/ which was used in this study. This work was supported by NASA Headquarters under the NASA Earth and Space Science Fellowship Program - Grant 80NSSC17K0339.

References

Baret, F., Houlès, V., & Guérif, M. (2007). Quantification of plant stress using remote sensing observations and crop models: the case of nitrogen management. *Journal of Experimental Botany,* 58(4), 869–880.

Brisson, N., Ruget, F., Gate, P., Lorgeou, J., Nicoullaud, B., Tayot, X., . . . Justes, E. (2002). STICS: a generic model for simulating crops and their water and nitrogen balances. II. Model validation for wheat and maize. *Agronomie*, 22, 69-92.

Combal, B., Baret, F., Weiss, M., Trubuil, A., Macé, D., Pragnère, A., . . . Wang, L. (2003). Retrieval of canopy biophysical variables from bidirectional reflectance: Using prior information to solve the ill-posed inverse problem. *Remote Sensing of Environment*, 84(1), 1-15.

Fang, H., Liang, S., Hoogenboom, G., Teasdale, J., & Cavigelli, M. (2008). Corn-yield estimation through assimilation of remotely sensed data into the CSM-CERES-Maize model. *International Journal of Remote Sensing*, 29(10), 3011-3032.

Greff, K., Srivastava, R. K., Koutník, J., Steunebrink, B. R., & Schmidhuber, J. (2017). LSTM: A search space odyssey. *IEEE Transactions on Neural Networks and Learning Systems*, 28(10), 2222 - 2232.

Houborg, R., McCabe, M., Cescatti, A., Gao, F., Schull, M., & Gitelson, A. (2015). Joint leaf chlorophyll content and leaf area index retrieval from Landsat data using a regularized model inversion system (REGFLEC). *Remote Sensing of Environment*, 159, 203-221.

Ines, A. V., Das, N. N., Hansen, J. W., & Njoku, E. G. (2013). Assimilation of remotely sensed soil moisture and vegetation with a crop simulation model for maize yield prediction. *Remote Sensing of Environment*, 138, 149-164.

Jin, Z., Azzari, G., & Lobell, D. B. (2017). Improving the accuracy of satellite-based high-resolution yield estimation: A test of multiple scalable approaches. *Agricultural and Forest Meteorology*, 247, 207-220.

Johnson, D. M. (2016). A comprehensive assessment of the correlations between field crop yields and commonly used MODIS products. *International Journal of Applied Earth Observation and Geoinformation*, 52, 65-81.

Koetz, B., Baret, F., Poilve, H., & Hill, J. (2005). Use of coupled canopy structure dynamic and radiative transfer models to estimate biophysical canopy characteristics. *Remote Sensing of Environment*, 95(1), 115 – 124.

Lancashire, P. D., Bleiholder, H., Van Den Boom, T., Langelüddeke, P., Stauss, R., Weber, E., & Witzenberger, A. (1991). A uniform decimal code for growth stages of crops and weeds. *Annals of Applied Biology*, 119(3), 561-601.

Lobell, D. B., Thau, D., Seifert, C., Engle, E., & Little, B. (2015). A scalable satellite-based crop yield mapper. *Remote Sensing of Environment*, 164, 324-333.

Machwitz, M., Giustarini, L., Bossung, C., Frantz, D., Schlerf, M., Lilienthal, H., . . . Udelhoven, T. (2014). Enhanced biomass prediction by assimilating satellite data into a crop growth model. *Environmental Modelling & Software*, 62, 437-453.

McInerney, D., & Kempeneers, P. (2014). Image (Re-)projections and Merging. *Open Source Geospatial Tools*, 99-127.

Morell, F. J., Yang, H. S., Cassman, K. G., Van Wart, J., Elmore, R. W., Licht, M., . . . Grassini, P. (2016). Can crop simulation models be used to predict local to regional maize yields and total production in the U.S. Corn Belt? *Field Crops Research*, 192, 1-12.

National Agricultural Statistics Service. (2017, December 4). *Surveys: Farm and Ranch Irrigation*. Retrieved from Guide to NASS Surveys: https://www.nass.usda.gov/Surveys/Guide_to_NASS_Surveys/Farm_and_Ranch_Irrigation/index.php

Sakamoto, T., Gitelson, A. A., & Arkebauer, T. J. (2013). MODIS-based corn grain yield estimation model incorporating crop phenology information. *Remote Sensing of Environment*, 131, 215-231.

Schlemmer, M., Gitelson, A., Schepers, J., Ferguson, R., Peng, Y., Shanahan, J., & Rundquist, D. (2013). Remote estimation of nitrogen and chlorophyll contents in maize at leaf and canopy levels. *International Journal of Applied Earth Observation and Geoinformation*, 25, 47-54.

Stackhouse, P. W., Westberg, D., Chandler, W. S., Zhang, T., & Hoell, J. M. (2017). *Prediction Of Worldwide Energy Resource (POWER) - Agroclimatology Methodology.* Hampton: NASA Langley Research Center.

Swain, S., Wardlow, B. D., Sunil, N., Rundquist, D. C., & Hayes, M. J. (2013). Relationships between vegetation indices and root zone soil moisture under maize and soybean canopies in the US Corn Belt: a comparative study using a close-range sensing approach. *International Journal of Remote Sensing*, 34, 2814-2828.

Thorp, K. R., Wang, G., West, A. L., Moran, M. S., Bronson, K. F., White, J. M., & Mon, J. (2012). Estimating crop biophysical properties from remote sensing data by inverting linked radiative transfer and ecophysiological models. *Remote Sensing of Environment*, 124, 224-233.

Weiss, M., Troufleau, D., Baret, F., Chauki, H., Prévot, L., Olioso, A., . . . Brisson, N. (2001). Coupling canopy functioning and radiative transfer models for remote sensing data assimilation. *Agricultural and Forest Meteorology*, 108(2), 113-128.

Weninger, F., Bergmann, J., & Schuller, B. (2015). Introducing CURRENNT: The Munich Open-Source CUDA RecurREnt Neural Network Toolkit. *Journal of Machine Learning Research*, 16, 547-551.

Yuping, M., Shili, W., Li, Z., Yingyu, H., Liwei, Z., Yanbo, H., & Futang, W. (2008). Monitoring winter wheat growth in North China by combining a crop model and remote sensing data. *International Journal of Applied Earth*

Observation and Geoinformation, 10(4), 426-437.

Zhang, L., Guo, C. L., Zhao, L. Y., Zhu, Y., Cao, W. X., Tian, Y. C., . . . Wang, X. (2016). Estimating wheat yield by integrating the WheatGrow and PROSAIL models. *Field Crops Research*, 192, 55-66.